Journal of Structural Geology 52 (2013) 148–162

Contents lists available at SciVerse ScienceDirect

Journal of Structural Geology

journal homepage: www.elsevier.com/locate/jsg

Spatial distribution of deformation bands in damage zones of extensional faults in porous sandstones: Statistical analysis of field data

Sylvie Schueller [a,*], Alvar Braathen [a,b], Haakon Fossen [a,c], Jan Tveranger [a]

[a] Centre for Integrated Petroleum Research (CIPR), Uni Research, P.O. Box 7810, 5020 Bergen, Norway
[b] University Centre in Svalbard, 9171 Longyearbyen, Norway
[c] Department of Geoscience/University Museum of Bergen, University of Bergen, P.O. Box 7803, 5020 Bergen, Norway

ARTICLE INFO

Article history:
Received 13 July 2012
Received in revised form
9 March 2013
Accepted 18 March 2013
Available online 11 April 2013

Keywords:
Fault damage zone
Deformation bands
Clustering
Width–throw relationship
Fault growth

ABSTRACT

The distribution of deformation bands in damage zones of extensional faults in porous sandstones has been analyzed using 106 outcrop scanlines along which the position and frequency of deformation bands have been recorded. The analysis reveals a non-linear relationship between damage zone width and fault throw, a logarithmic decrease in deformation band frequency away from the fault core, as well as a fractal spatial distribution associated with clustering of the deformation bands. Furthermore, damage zones appear wider in the hanging wall than in the footwall, although the deformation band density is similar on both sides. Statistical trends derived from the database imply that fault growth in porous sandstones can be considered as a scale invariant process. From an initial process zone, the damage zone grows by a constant balance between the development of new deformation bands in the existing damage zone and the creation of new bands outside. Moreover, as the width of the damage zone increases throughout the active lifetime of a fault, the distribution of the deformation bands in the damage zone remains self-similar. Hence band distribution and damage zone width for seismically mapped faults can be predicted from the relationships found in this paper.

1. Introduction

Faults are commonly described as the association of two main architectural elements: a central fault core which accommodates most of the displacement and a surrounding fault damage zone (Wallace and Morris, 1979; Jamison and Stearns, 1982; Chester and Logan, 1987; McGrath and Davison, 1995; Caine et al., 1996; Beach et al., 1999; Shipton and Cowie, 2001, 2003; Fossen et al., 2005; Braathen et al., 2009). The fault damage zone is thus the volume of deformed rocks that results from initial process zone development and subsequent slip surface initiation, propagation, and linkage or interaction in the fault zone (Peacock et al., 2000; Kim et al., 2004; Fossen, 2010). This envelope of deformed rocks is of great interest in faulted reservoirs and aquifers, since its intrinsic characteristics and the distribution of small-scale damage structures is seen to influence fluid flow in a hydrocarbon or hydro reservoir setting. Further, the rocks contained within this envelope possess mechanical properties that differ from those of the pristine host rock.

Damage zone geometries have been studied through structural maps, detailed cross sections and microstructural analyses of deformation mechanisms (Jamison and Stearns, 1982; Chester et al., 1993; Antonellini and Aydin, 1994; McGrath and Davison, 1995; Schulz and Evans, 1998; Chester et al., 2004; Fossen et al., 2005; Johansen and Fossen, 2008). However, due to the multiplicity of parameters that can affect fault damage zone geometry, such as lithology and associated diagenesis, rheological stratification or inherited fault array geometry (Johansen et al., 2005; Childs et al., 2009; Braathen et al., 2009), the internal structure and evolution of damage zones are not fully understood.

In this paper, we analyze damage zone geometry through the study of deformation band distribution in highly porous sandstones (Fig. 1). Damage zones in porous sandstones form by growth of deformation bands prior to the establishment of a slip surface (e.g., Aydin and Johnson, 1978, 1983; Underhill and Woodcock, 1987; Mair et al., 2000; Rotevatn and Fossen, 2011; Fig. 2). In contrast, damage zones in low-porosity and non-porous rocks grow by fracture formation. Slip surfaces (secondary to the main fault) are found in damage zones in both porous and non-porous rocks. However, in porous rocks, they are scarce and often associated with zones of densely packed deformation bands

* Corresponding author. Present address: IFP Energies nouvelles, 1&4 Avenue de Bois-Préau, 92852 Rueil-Malmaison Cedex, France.
E-mail address: sylvie.schueller@ifpen.fr (S. Schueller).

0191-8141/$ – see front matter © 2013 Elsevier Ltd. All rights reserved.
http://dx.doi.org/10.1016/j.jsg.2013.03.013

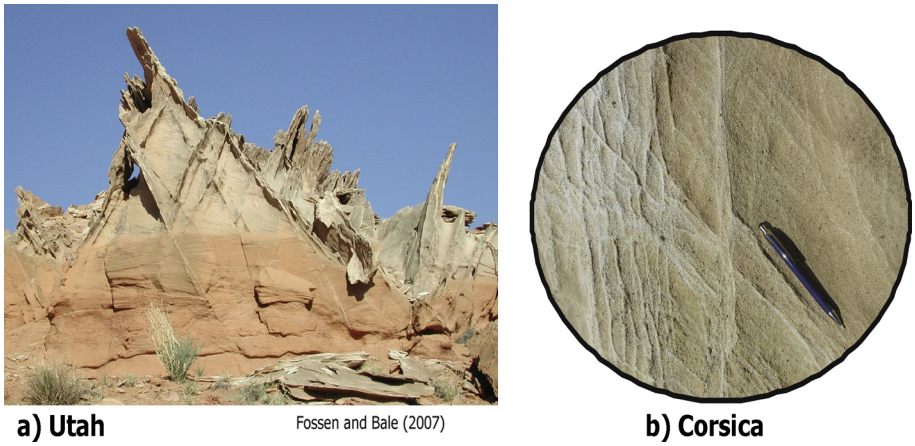

Fig. 1. Illustrations of a) a damage zone in Utah (from Fossen and Bale, 2007) displaying two distinct deformation band sets, and b) deformation bands in porous sandstone from the Aleria basin of Corsica (France).

(Aydin and Johnson, 1978; Antonellini et al., 1994; Shipton and Cowie, 2001; Johansen and Fossen, 2008). Fractures that may form in damage zones due to late fault reactivation, typically after substantial lithification and loss of porosity, are not considered in this work.

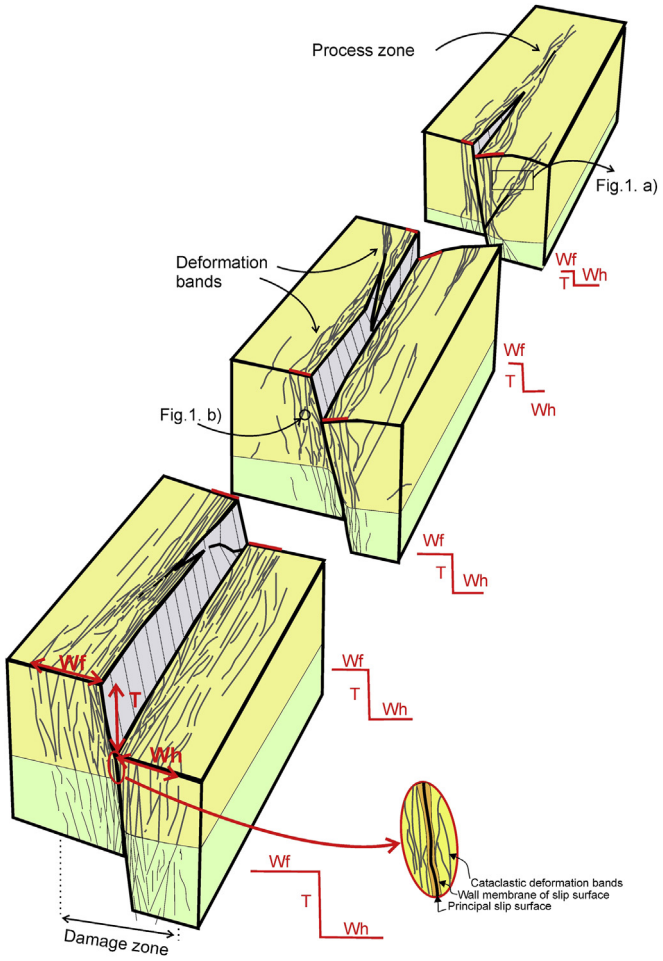

Fig. 2. Illustration of extensional fault in porous sandstone succession, showing a principal slip surface accommodating nearly all displacement and deformation structures (deformation bands and fractures) in footwall and hanging wall damage zones. *Wf* = width of the footwall damage zone; *Wh* = width of the hanging wall damage zone; *T* = throw.

Deformation bands are millimeter-thick structures that result from strain localization processes in highly porous granular media. They are characterized by grain reorganization due to grain sliding, rotation and/or fracturing associated with dilation, shear and/or compaction mechanisms. Different types of deformation bands exist: cataclastic bands, disaggregation bands, phyllosilicate bands, and solution and cementation bands (Fossen et al., 2007). The formation of these different types of deformation bands appears to depend on a large number of factors, such as the porosity of the host rock, which is fundamental for grain re-organization and stress concentration at grain contacts (Flodin et al., 2003; Johansen et al., 2005), but also on grain sorting, grain roundness, burial depth, cementation and state of stress (Antonellini and Pollard, 1995; Menendez et al., 1996; Mair et al., 2000; Hesthammer and Fossen, 2001; Schultz and Siddharthan, 2005). The most common deformation bands are cataclastic bands, as described by Aydin (1978) (Fig. 1), which is nearly exclusively the type of bands covered in this study. Their individual offset is generally not greater than a few centimeters even though they can reach more than 100 m in length (Fossen and Hesthammer, 1997); their height is commonly limited by the layer thickness. Compaction within cataclastic bands causes a reduction in porosity and permeability as compared to the host rock (e.g., Fisher and Knipe, 2001; Fossen et al., 2007). It has, however, been observed that individual bands display high lateral variability in their petrophysical properties, which would prevent bands from acting as impermeable barriers to fluid flow (Fossen and Bale, 2007; Torabi and Fossen, 2009).

Deformation bands in damage zones can occur solitary or clustered (Aydin and Johnson, 1978; Johansen and Fossen, 2008). Deformation characteristics within a damage zone are important for stress distributions as well as fluid flow in reservoirs; the latter depending on the vertical and horizontal continuity and connectivity of the bands as well as on their geometrical arrangement (Kolyukhin et al., 2009). For instance, deformation bands might reduce the sweep in the most permeable sandstone layers and thereby counteract the expected early water breakthrough in such intervals at wells (Fossen and Bale, 2007). From another point of view, the intrinsic geometry of damage zones can be connected to the processes of fault growth, giving insight into fault growth mechanisms.

Damage zones in fault branch points or relay zones tend to be wider than damage zone of isolated, straight or simple fault segments. Relay zones also show a wider range in orientation of deformation bands and fractures (Fossen et al., 2005). For simplicity, our study of damage zones is focused on simple fault

Table 1
Database overview. The number of scanlines is given for each throw encountered at a certain location. Bold numbers represent the total number of scanlines for the corresponding location.

	Location	Number of scanlines	Fault throw (m)	Lithology SST: Sandstone	References used
Sinai, Egypt	Tayiba Mines	**8**	100	Fluvial/deltaic SST	CIPR fieldwork
	Wadi El Khabouba	**9**: 1; 1; 1; 6	15; 20; 100; 140	Fluvial SST	Beach et al., 1999; CIPR fieldwork
	Wadi Matulla	**6**: 2; 2; 2	3.1; 3.5; 50	Fluvial and aeolian SST	Beach et al., 1999; Ehrlich, 2003
	Western Sinai	**9**:1; 2; 2; 1; 1; 1; 1	10; 30; 50; 75; 100; 200; 2000	Fluvial SST	Knott et al., 1996
	Wadi Araba	**2**	3	Fluvial SST	Du Bernard et al., 2002
	Gebel Hazbar	**2**	5	Fluvial SST	Du Bernard et al., 2002
	Naqb Budra	**1**	30	Fluvial SST	Du Bernard et al., 2002
	Gebel Samra	**1**	2500	Fluvial SST	Du Bernard et al., 2002
	Wadi Isaila	**1**	20	Fluvial and aeolian SST	CIPR fieldwork
	Close to Wadi Baba	**9**: 8; 1	14; 200	Fluvial SST	CIPR fieldwork
	Thal fault	**2**	2000	Fluvial SST	CIPR fieldwork
Utah	Delicate Arch	**7**: 3; 2; 1; 1	20; 40; 100; 150	Aeolian SST	Antonellini and Aydin, 1994
	SE of Dead Horse Creek, near Goblin Valley State Park entrance	**9**: 1; 4; 4	2.02; 5; 15	Aeolian medium to fine grained SST – interdune deposits	Fossen et al., 2005; CIPR fieldwork
	Bartlett fault	**18**: 2; 16	15; 200	Aeolian medium to fine grained SST – interdune deposits	CIPR fieldwork
	Mill Canyon	**2**	10	Medium to coarse Aeolian SST	Johansen and Fossen, 2008
	San Rafael Desert	**14**: 1; 10; 1; 2	1.7; 1.9; 12; 15	SST/siltstone	Johansen and Fossen, 2008
England	Northumberland	**1**	140	Fine-medium grained Aeolian SST	Knott et al., 1996
Corsica	Aleria basin	**3**: 1; 1; 1	6; 8; 20	Medium to coarse grained SST (fluvial to shallow marine)	CIPR fieldwork
Svalbard	Billefjorden	**1**	1200	Carboniferous SST	CIPR fieldwork
Netherlands	Roer valley	**1**	0.2	Fluvial sands	Bense et al., 2003

segments or segments without obvious mechanical interaction with other fault segments.

We here present an analysis of damage zones of extensional faults in highly porous sandstone. Our study centers on quantitative characterization of fault damage zones through the spatial distribution of deformation bands and how these evolve in response to fault displacement. Key characteristics, including damage zone/fault size scaling relationships, were extracted from an extensive database of field observations. The focus is on the relationships between the width of the damage zone, the distribution of bands within the damage zone, and the fault throw.

2. Database of field observations

In order to establish a database on damage zone geometry in porous sandstone successions, detailed fault damage zone scanlines were acquired. A database of 106 scanlines was compiled from outcrop observations. We consider this database sufficiently large and representative to allow general conclusions to be drawn for porous sandstones.

2.1. Host rock, faults and damage zones

The database was partly compiled from published sources (Antonellini and Aydin, 1994; Knott et al., 1996; Beach et al., 1999; Gjessen, 2001; Du Bernard et al., 2002; Bense et al., 2003; Ehrlich, 2003; Johansen and Fossen, 2008) and partly from field data collected by the Department of Earth Science (University of Bergen, Norway) and UNI Centre for Integrated Petroleum Research (UNI CIPR). The bulk (94%) of the data derives from mainly fluvial Nubian Sandstone in Sinai (Egypt) and overall aeolian Entrada and Navajo Sandstones in Utah (USA) (Table 1). Fault throws range from 1 to 2500 m, with the majority of data corresponding to throws between 100 and 200 m (Table 1 and Fig. 3). All faults are normal faults, with 60% of the scanlines recorded in the footwall, and 40% in the hanging wall. The host rock lithologies are highly porous, coarse- to fine-grained sandstones (Table 1), with a few data from very fine-grained sandstones. In order to constrain the number of uncontrollable factors affecting the dataset, we have limited our study to the analysis of damage zones surrounding individual fault segments. Accordingly, damage zones situated in relay zones have been discarded.

2.2. Data collected for each damage zone

In this study we handle footwall and hanging wall data separately. Ideally these should be considered together, however, both footwall and hanging wall damage zones are rarely exposed for individual faults. Hence, the expression “damage zone width”, as used here, corresponds to what has been called the “damage zone half width” by some authors (e.g., Hesthammer and Fossen, 2001; Shipton et al., 2006; Fossen et al., 2007; Fossen and Bale, 2007; Lockner et al., 2009; Powers and Jordan, 2010) and thus half the damage zone discussed by others (e.g., Shipton and Cowie, 2001;

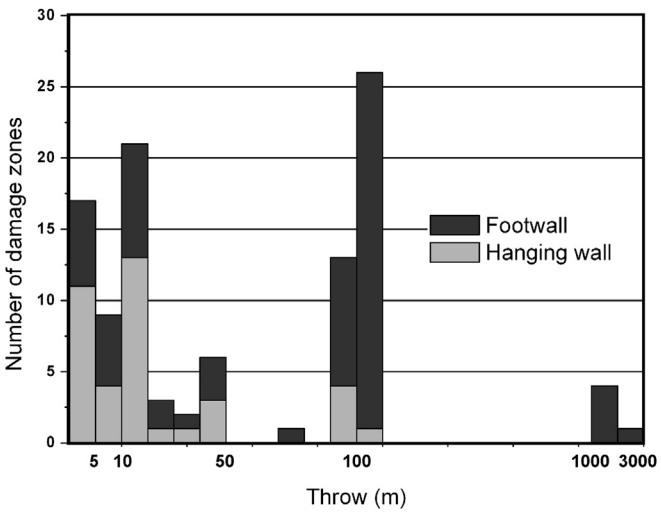

Fig. 3. Distribution of damage zones in the database as a function of fault throw, distinguishing between hanging wall and footwall data.

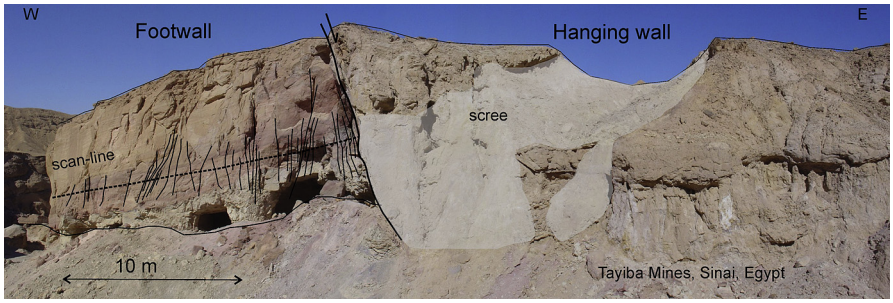

Fig. 4. Example of outcrop with location of scanline from the quarry and mine system in Wadi el Hommur (Malha Formation, Nubian Sandstone), Sinai, Egypt. Deformation band frequencies along scanlines were recorded only in the footwall in this case (scree-covered slope in the hanging wall).

Childs et al., 2009; Faulkner et al., 2011). Fault throw was recorded at the position of each scanline, disregarding (but noting) any additional displacement caused by ductile drag. Also the width of the damage zone along the scanline and the deformation band frequency (number of deformation bands per meter) were recorded. In this study, a deformation band refers to a ~1-mm thick tabular zone characterized by cataclastic deformation. Clusters of deformation were not considered as a whole; we tried to individualize the different bands within the clusters, i.e., each individual band was counted. Additional information, such as drag folding, layer thickness, and the host rock permeability were recorded when available. All scanlines are oriented perpendicular to fault strike and follow single stratigraphic layers (Fig. 4). In total, 106 1D scanlines (Table 1) from damage zones of extensional faults in porous sandstones are analyzed in this study. For some scanlines (28 out of 106), the precise positions of individual deformation bands along the scanline were recorded, offering essential information on the clustering of the deformation bands. The majority of the observed structures strike more or less parallel to their associated main fault (see Aydin, 1978; Johnson, 1995; Berg and Skar, 2005; Johansen and Fossen, 2008). Dip of the deformation bands ranges from ±50 to ±80° with respect to bedding.

2.3. Uncertainties in the dataset

Field observations are often hampered by scree-cover, leading to gaps in datasets along the scanlines. In the database, 22 scanlines (out of 106) lack data either at the beginning, in the middle or at the end of the damage zone. These incomplete scanlines were used when possible for characterizing the spatial organization of the bands, or, where the ends were recorded, for estimating the width of the damage zone, but were not included in calculations of average deformation band density. Further, there is an uncertainty related to fault throw. For small faults with up to 10 m throw, uncertainty is in the order of centimeters. For very large faults, uncertainty can be up to a few hundred meters, since the throw cannot necessarily be measured directly at the scanline location and must be deduced from cross-sections.

Defining damage zone width largely depends on how the fault core and the background deformation intensity are defined. In most of the scanlines (CIPR fieldwork; Table 1), the inner boundary of the damage zone is defined as the boundary between clearly visible original layering and the more chaotic fault core characterized by fault gouge and very low degree of layer continuity. The outer boundary of the damage zone is defined by the first occurrence of a 3 m interval along the scanline devoid of deformation band. The background density of the studied faulted sedimentary succession was generally less than 1 deformation band per meter.

3. Damage zone characterization

Our damage zone characterization includes damage zone width, fault throw, average density of deformation bands within the zone and the distribution of bands across the damage zone.

3.1. Description of deformation band density

Fig. 5 shows a graph of deformation band density versus distance across the footwall side of the damage zone of a fault with ~100 m throw (fault displayed in Fig. 4). In this case the background deformation intensity is lower than one deformation band per meter. Since the density does not decrease linearly with distance from the fault core, the precise location at which the background density is reached can be subjective. In this study, we apply a more objective definition of the damage zone width; a criteria that opens for comparison of different fault damage zones.

The width is expressed as *Wx* (in meters), where *x* represents the deformation band density reached at the distance *Wx* from the fault core, either in the footwall or the hanging wall. For example, *W*5max is the outermost location at which the band frequency is at or above 5 m^{-1}, while *W*5min is defined as the minimum distance from the fault core where the frequency first drops below 5 m^{-1}.

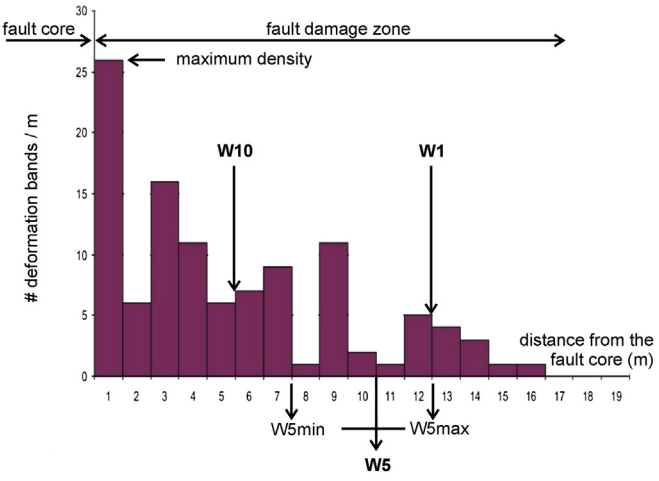

Fig. 5. Frequency graph illustrating different ways of defining the damage zone width. *W*5min is the distance from the fault core in which the frequencies are consistently higher than 5 deformation bands per meter. *W*5max is the distance beyond which the frequencies are consistently lower than 5 deformation bands per meter. *W*5 is the distance corresponding to an average of 5 deformation bands per meter. *W*10 and *W*1 are the distances corresponding to an average of 10 and 1 deformation band(s) per meter, respectively. The example is taken in the footwall side of the fault with a 100 m throw situated in the Wadi el Hommur Mines (Egypt) (same fault as shown in Fig. 4).

The arithmetic mean between *W*5max and *W*5min corresponds to *W*5 (Fig. 5); *W*5 is the distance from the fault core to the point at which the average frequency of deformation bands is 5 m^{-1}. Other average widths, for example corresponding to band frequencies of 10 m^{-1} (*W*10) or 1 m^{-1} (*W*1), can be defined in a similar manner. However, taking one deformation band per meter as a limit for the width of the damage zone can be very sensitive to the decision made in the field regarding the required length of the scanline. For example, in Fig. 5, one deformation band might be found at 25 m from the fault core, which would change drastically the value of *W*1. A frequency of 10 deformation bands per meter corresponds to a rather high frequency and is not necessarily encountered in all the damage zones. *W*5 was chosen as the standard width measure for the analysis since it appeared as one of the statistically most robust values encountered in nearly all the damage zones analyzed in this work, even the ones associated with a fault throw of around 1 m. The fact that deformation band zones form as fault precursors (e.g., Aydin and Johnson, 1978; Shipton and Cowie, 2001) is an important reason why the *W*5 criterion works so well even for small faults, hence a different choice of *Wx* may be preferable for non-porous or low-porosity rocks.

3.2. Width–throw relationship

In this study, *W*5 (see above) is used to define damage zone width. A plot of damage zone width versus fault throw reveals a positive but non-linear correlation. The best fit function established is a power-law relationship (Fig. 6). The confidence intervals and prediction belts have been calculated with 95% confidence. The confidence belt around the regression line indicates that, for a given throw, the true value of the width should be located within this belt, for a given data set. The prediction belt defines, for a given throw, the interval within which a new observation of width should be found if this new observation belongs to the same statistical population as the data set used to define the regression line. This belt is larger than the confidence belt because the variance associated to draw a new point is added to the variance of the existing data set. The high variability of damage zone width is emphasized by the prediction belt spanning more than two orders of magnitude along the *y*-axis.

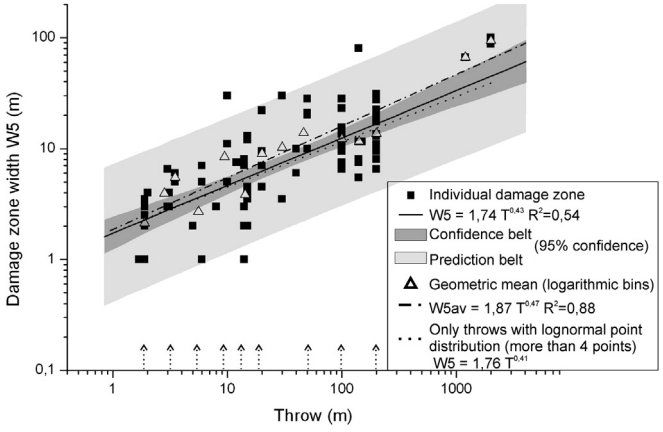

Fig. 6. Damage zone width (*W*5) as a function of throw. The best fit (black solid line), the confidence and prediction belts have been calculated on the individual data point set. The geometric means have been calculated for different groups of throw using a logarithmic binning along the *x*-axis. The dotted trend is obtained using only the groups of throw represented by more than 4 damage zones and presenting a lognormal distribution of the widths. Each point is weighted by the variance of its group.

A positive correlation between fault throw and damage zone thickness is well established in most of the existing literature (e.g., Beach et al., 1999; Shipton and Cowie, 2001; Johansen and Fossen, 2008; Childs et al., 2009; Savage and Brodsky, 2011), although the published data come from different tectonic settings and lithologies, and definitions of the damage zone are inconsistent. Statistical analysis of our own damage zone data from highly porous sandstones in the extensional regime shows that several trends can be defined. Three of these are shown in Fig. 6. Throws of 100–200 m are overrepresented in our database (Fig. 3), and one can argue that more weight is given to the damage zones corresponding to these throws when using individual data and the least square approximation (defining the black solid line trend in Fig. 6). In order to avoid this type of bias, values for throw were grouped through a logarithmic binning along the *x*-axis. Since the majority of these groups shows a logarithmic distribution of the damage zone widths, the geometric mean of the widths was calculated for each group (represented by an empty triangle in Fig. 6) and then a new trend using the least square approximation was calculated (black dash-dot line in Fig. 6). The best fit is still a power-law, although with a slightly higher exponent than the one calculated for individual (unbinned) data, since the large throws (being underrepresented) now have the same weight as the 100 and 200 m fault throws. On the other hand, groups of data containing only two points might not be considered representative. An alternative approach is therefore only to use bins with more than 4 data points that show a logarithmic distribution. These groups of points, related to specific ranges of throw, are indicated by an arrow along the *x*-axis in Fig. 6 (each arrow indicating the average throw of each group or bin). Note that the faults with large throw (>1000 m) are discarded when using this method. The resulting trend (dotted line in Fig. 6) is calculated from the points in these groups weighted by the variance of the corresponding group. Even if the very large throws are not considered, the trend still falls inside the confidence belt obtained for the whole database.

A power law ($W = aT^b$, where *W* is the width of the damage zone, and *T* the throw of the corresponding fault) seems thus to be the most robust description of the relationship between the width of the damage zone and the throw. For our dataset, the exponent "*b*" has a value between 0.4 and 0.5 and the value "*a*" (the ordinate for a throw equal to 1 m) ranges between 1 and 2.5 (for *W*5 values). The various ways of calculating the width (*W*10, *W*5 and *W*1; see above) hardly change the trend (slope) between the width and the fault throw. The best-fitting trends (yielding the highest values for R^2) are power law functions with an exponent varying between 0.44 and 0.46 (Fig. 7). However, the parameter "*a*" depends on the

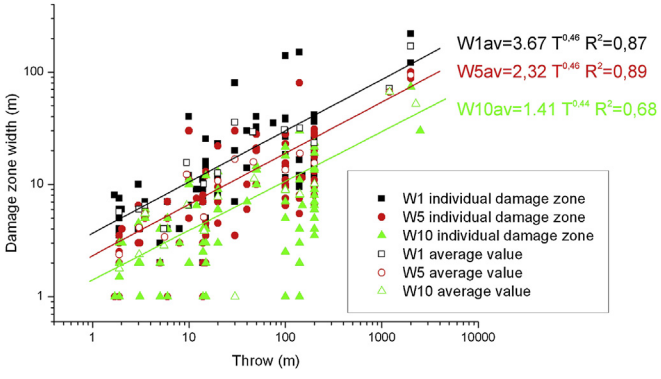

Fig. 7. Damage zone widths as a function of throw. The represented widths are *W*10, *W*5, *W*1. The trends are calculated using the geometric mean of the widths for the different throw groups.

definition of damage zone width, and increases when changing the standard width from *W*10 to *W*1 (Fig. 7). The quantitative results, yielding a slope of ~0.5, are in good agreement with the results of Beach et al. (1999). On the other hand, data presented by Shipton and Cowie (2001) for fault throws ranging from 0 to 25 m, display a linear relationship (i.e., $b = 1$). However, the limited range of throw in their data set is insufficient to extrapolate the width–throw relationship to larger throws. A composite non-linear trend could be modeled as a combination of a linear trend for low throws with a decreasing slope toward higher fault throws. However, we here prefer the power law because it describes the relationship over a wider range of throws by means of a simple relationship that fits our current database quite well.

The trends presented here (Figs. 6 and 7) are valid for throws ranging from 1 to 2500 m. Extrapolation of the curve to lower values of throw is not possible, since a fault tip process zone, i.e. the zone of deformation bands ahead of the fault tip (e.g., Shipton and Cowie, 2001; Rotevatn and Fossen, 2011), is established before the development of the slip plane itself (e.g., Scholz et al., 1993; Fossen et al., 2007). The width of the damage zone, when the fault throw approaches zero, is thus finite: a few meters (~3 m) can be expected if we consider the value given by Shipton and Cowie (2001), which would represent the *W*1max value for the Navajo Sandstone in their study area. The critical width of the process zone before the slip surface initiation depends probably on a large number of lithological parameters, including porosity, grain size, mineralogy, sorting, layer thickness and local stress conditions (Fossen et al., 2007; Johansen and Fossen, 2008).

3.3. Average density of deformation bands

The *average density* of deformation bands in a damage zone, "*D*", is defined by the ratio between the total number of deformation bands present in the damage zone up to a certain distance *W*, divided by the distance *W*:

$$D = \left[\sum_{0}^{W}(\text{number of deformation bands})\right] \Big/ W$$

For instance, *D*5 is the average deformation density calculated up to the distance *W*5 (Fig. 5 for the definition of *W*5). The average density is a proxy for the degree of deformation in the damage zone either in the footwall or the hanging wall. Fig. 8A shows the average density *D*5 calculated for the available damage zones as a function of the fault throw. Plotted data points show no dependence between the average density of deformation bands and the throw. The best fit presented in Fig. 8A indicates a slight decrease in density as a function of throw; nevertheless this trend is not significant since the fitting factor is very low ($R^2 = 0.026$). Thus as the number of deformation bands grows, *W*5 increases proportionally to keep the *D*5 sub-constant. So, as *W*5 doubles, so does the number of deformation bands, and the deformation band density remains more or less constant over time in the range $15 \pm 9\ m^{-1}$ (Fig. 8A).

The *maximum density* of deformation bands is also independent of the throw on the fault. The maximum density is here defined as the maximum frequency of deformation bands per meter as observed in a scanline (Fig. 5). Fig. 8B shows the maximum density observed in the different damage zones as a function of the fault throw. The best fitting trend indicates a slight linear increase of the maximum density with increasing throw, but as for the average density, this trend is not significant since the fitting factor R^2 is 0.077.

The results shown in Fig. 8 agree with previous findings from the Entrada Sandstone in Utah (Johansen and Fossen, 2008), suggesting that there may be a certain density threshold in highly porous sandstones, i.e. a maximum band density that cannot be exceeded. This threshold, which is strongly influenced by the petrophysical properties of the host rock as well as the microscale mechanisms operative in the deformation bands, is probably closely related to the density of deformation bands and width of the process zone at the time of fault (slip surface) initiation.

3.4. Spatial distribution of the deformation bands

3.4.1. Logarithmic decrease

Decrease of the concentration of subsidiary structures away from a fault is a common feature generally seen in most lithologies, including sandstones (Knott et al., 1996; Vermilye and Scholz, 1998; Beach et al., 1999; Fossen and Hesthammer, 2000; Hesthammer and Fossen, 2001; Shipton and Cowie, 2001; Du Bernard et al., 2002; Berg and Skar, 2005; Johansen and Fossen, 2008), limestones (Micarelli et al., 2003), mudstones (Savage and Brodsky, 2011), and crystalline rocks (Chester et al., 2004). In order to quantify this decrease in our database, different models have been tested: linear, exponential, logarithmic and power-law. Considering fitting factors R^2 above 0.5, the logarithmic model appears to be the best fitting model for 81% of the damage zones of the database. The logarithmic model is defined as $Y = A + L\ln(X)$, with *Y* representing frequency of deformation bands per meter and *X* the distance from the fault core (Fig. 9A).

As opposed to functions that asymptotically approach zero or a constant value, the logarithmic decay function is not valid for an

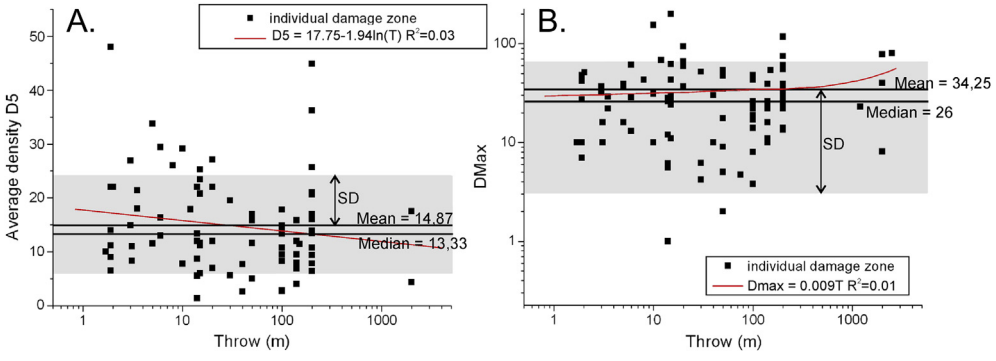

Fig. 8. A) Average density of deformation bands, *D*5, in the damage zone as a function of fault throw. B) Maximum density of deformation bands, *D*max, recorded in the damage zones as a function of throw. In both figures, the gray shading outlines the variability of the density values by considering fluctuation corresponding to the standard deviation around the mean value (the standard deviation for the average density *D*5 is 9.05 and for the maximum density: 31.49). The best fitting trends are given for information but have no statistical significance since the fitting factors are very low.

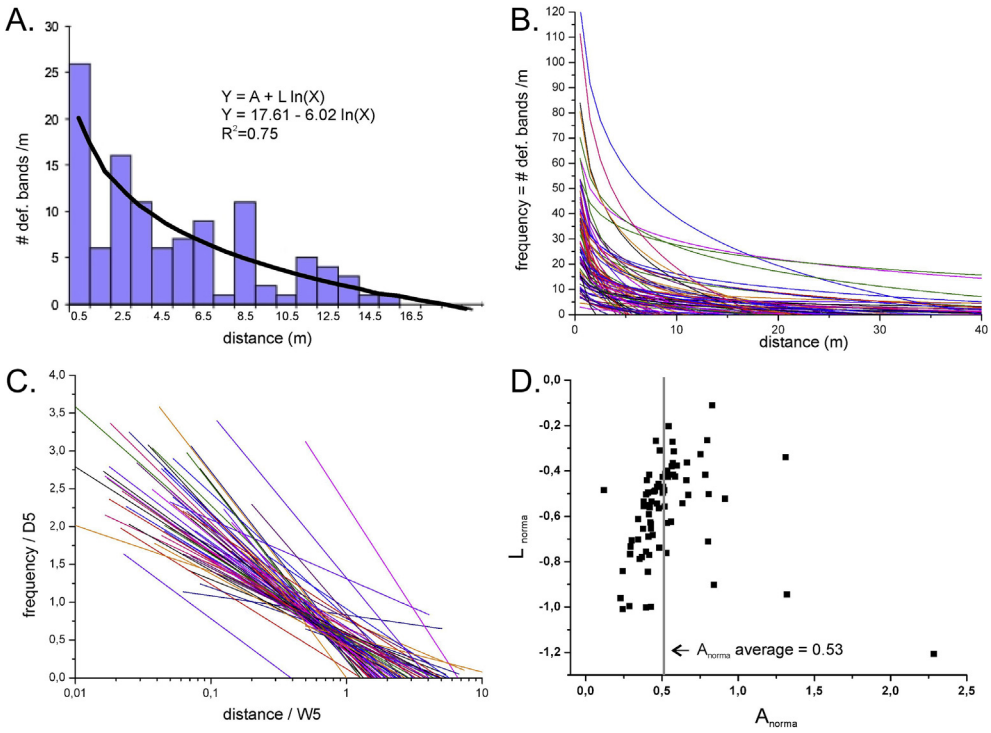

Fig. 9. A) Frequency graph for a fault (same fault as in Fig. 4) with 100 m throw. The decrease of the frequency of deformation bands away from the fault core is best represented by a logarithmic fit ($Y = A + L\ln(X)$, with Y the number of deformation bands per meter and X the distance from the fault core); B) Logarithmic fit for all the frequency graphs from the database; C) Normalization of all the frequency graphs: The frequency (i.e. number of deformation bands per meter) is divided by $D5$ and the distance is normalized by $W5$ (see 3.1 and 3.3 for the definition of $W5$ and $D5$); D) A_{norma}–L_{norma} plot: $A_{norma} = (A + L\ln(W5))/D5$ and $L_{norma} = (A/D5 - A_{norma})/\ln(1/W5)$. Each point corresponds to one damage zone.

infinite range of distances from the fault core, but only for distances ranging between zero and the damage zone width. Beyond the damage zone width, the deformation band density corresponds to the background density. The logarithmic model allows us to describe the decrease in deformation band frequency by means of only the two parameters A and L. So, in order to forecast the position of the outer margin of the damage zone, the logarithmic function can be used to calculate its theoretical width as well as the average deformation band density at a certain distance from the fault core. For example, knowing the A and L parameters, the damage zone width $W5$ (the distance from the fault core to the point at which the average frequency of deformation bands is 5 m^{-1}) will be defined as $W5 = \exp((5 - A)/L)$.

Fig. 9B shows all logarithmic graphs of deformation band frequency in our database. A large range of "A" and "L" values can be observed. The frequency graphs have thus been tentatively normalized: the distance has been divided by $W5$ and the frequency has been divided by $D5$ (the average density of deformation bands at a distance of $W5$) (Fig. 9C). Two new normalized parameters have been calculated on the normalized frequency graphs: A_{norma} $(= (A + L\ln(W5))/D5)$ and L_{norma} $(= (A/D5 - A_{norma})/\ln(1/W5))$.

Fig. 9D displays the A_{norma} and L_{norma} values for all the damage zones of the database. The A_{norma} values are more or less gathered around the average value of 0.53, while the L_{norma} values remain scattered.

3.4.2. Clustering of deformation bands

One characteristic feature of damage around normal faults in porous sandstones is the clustering of deformation bands. As illustrated in Fig. 9A, the deformation band frequency does not decrease monotonously along the logarithmic decay, but exhibit clustering even far from the fault core. In general, deformation band frequencies tend to peak near the center of the clusters (Johansen and Fossen, 2008).

In order to characterize the clustering of the deformation bands, the precise position of each individual deformation band was recorded along some of the scanlines. A correlation analysis is regarded as an efficient method to identify scaling properties and to precisely describe the spatial distribution of fracture densities (Vicsek, 1989). Our correlation analysis is based on the calculation of the correlation integral by using a modified version of the discretized equation of Grassberger and Procaccia (1983):

$$C(r) = \frac{2}{N \times (N-1)} \sum_{i<j} \Theta\left(r - |x_i - x_j|\right) \approx r^{Dc}$$

where N is the total number of deformation bands in the scanline; x is the position of the deformation band in the scanline (distance from the fault core); r is the maximum tested distance between two deformation bands along the scanline. Θ is the Heaviside function, which is defined as $\Theta(x) = 1$ if $x > 0$ and $\Theta(x) = 0$ if $x < 0$. Dc is the correlation dimension or fractal dimension. The correlation function is a measure of the number of pairs of deformation bands that display a spacing ($x_i - x_j$) smaller than the distance "r". In our calculations, r varies from 1 mm to the scanline length. The correlation integral is then plotted as a function of the distance r in a log–log diagram (Fig. 10A). The slope of the correlation integral calculated with a linear regression corresponds to the exponent Dc of the power law. For a linear distribution (such as 1D scanlines), Dc can vary between 0 (highly clustered deformation bands and thus localized at a single point) and 1 (deformation bands homogeneously distributed in the damage zone) (Fig. 10B). The value of Dc thus quantifies the degree of deformation band clustering in the damage zone.

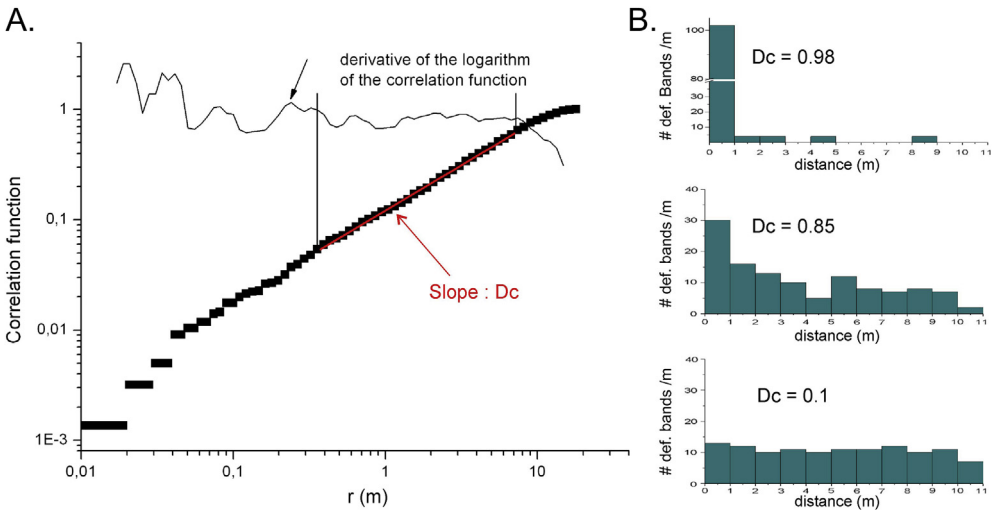

Fig. 10. A. Correlation analysis with correlation function as a description of the distance *r* between the deformation bands. If the organization of the deformations bands is fractal, the correlation function presents a linear trend in a log–log diagram and its slope is the correlation dimension Dc. In order to define the range over which Dc can be calculated, the 5 points derivative curve of the correlation function is calculated. B. Theoretical examples of clustering characterized by the correlation dimension Dc and their corresponding frequency graph. Dc = 0.85 is the distribution closest to the ones observed in nature.

For practical use, a 5-point derivative function is calculated (e.g. Fig. 10A), based on the valid range of distances over which the correlation dimension can be calculated; the valid range of distances is defined where the derivative function is stable and constant. The range over which the correlation dimension can be calculated for a single scanline can vary. The correlation dimension itself contains an inherent error of determination equal to ±0.05 according to Du Bernard et al. (2002). Moreover, natural systems are not expected to be exactly deterministic fractal (Du Bernard et al., 2002), because the fracturing or deformation process can introduce some mechanical or petrophysical constraints in the system (i.e. local modifications of the mechanical properties of the rock) leading to some variability of the distribution of the structures.

Fig. 11 shows the computed correlation dimension Dc as a function of the fault throw. Calculations using the database indicate an average correlation dimension Dc of 0.837 with a standard deviation of ±0.062. When the correlation dimension is calculated over a scale range spanning two orders of magnitude, the power law distribution of deformation bands in the damage zone is recognized. When the correlation dimension is valid only for one order of magnitude, other distributions cannot be excluded (Bonnet et al., 2001). In our case, from the 31 scanlines that were available for the clustering analysis, 54% of Dc values were defined on one order of magnitude length range, 42% on two orders of magnitude, and 4% could be defined on a three orders of magnitude length range.

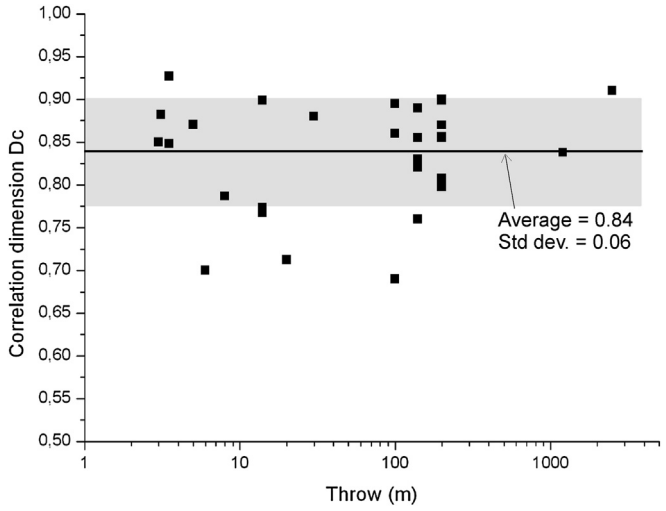

Fig. 11. Correlation dimension Dc as a function of the fault throw for 31 faults from our database. Each point corresponds to a damage zone. Dc appears independent of the throw, so the average Dc is 0.84 with a standard deviation equal to 0.06.

Since the correlation dimension Dc can be defined, the spatial organization of deformation bands should be the same at different scales. In order to test for scale invariance, the scanline can be binned so that clustering analysis can be performed on the different parts. Scale invariance then implies that the same correlation dimension should be found for each data subset. One of the drawbacks of clustering analysis is the need for numerous data points (large number of deformation bands) to establish representative results. The test was thus performed on a large fault (throw larger than 1200 m) with a damage zone width (*W*1) of 68 m. The correlation dimension was calculated first on the total width of the damage zone and then only on the first half part of the zone. Dc for the whole damage zone is equal to 0.8465, whereas Dc for the first half part is equal to 0.8379. This confirms the scale-invariant nature of the deformation band distribution, at least for this particular case.

One striking aspect of Fig. 11 is that Dc seems to be independent of the throw of the fault and can therefore be expected to be constant throughout the fault growth history. This result is in accordance with the work by Du Bernard et al. (2002), implying that damage zone growth is a scale-invariant process.

4. Factors influencing the damage zone geometry

The large variability of density and width values cannot be explained only by the displacement accumulated along the fault. Some attempts have been made to separate the data according to parameters such as the hanging wall vs. footwall side of the fault, fault-related folding of layers, depth of faulting, and petrophysical properties of the host rock.

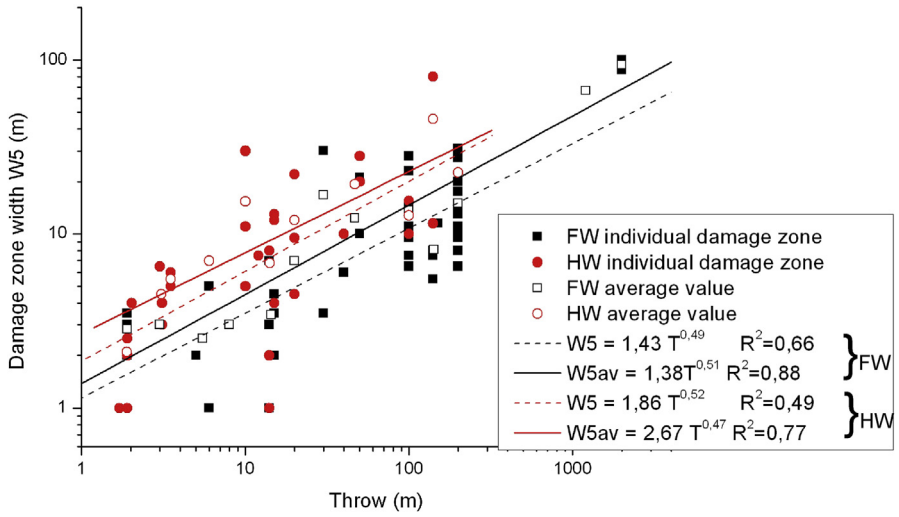

Fig. 12. Damage zone width (*W*5) in hanging wall and footwall as a function of the fault throw. Damage zones in the hanging wall are statistically wider than the damage zones in the footwall.

4.1. Hanging wall vs. footwall location

Asymmetric damage on each side of a fault is often reported or assumed in the literature (e.g., Cloos, 1968; McClay and Scott, 1991; Aarland and Skjerven, 1998; Withjack et al., 1995; Fossen and Hesthammer, 1998; Du Bernard et al., 2002; Berg and Skar, 2005; Brogi, 2008; Dor et al., 2006, 2008). To further test this assumption, the data have been separated into damage zones belonging to the footwall or hanging wall, which shows significant influence on the width–throw relationship (Fig. 12). For a similar throw, hanging wall damage zones are, in general, wider than footwall damage zones. In order to statistically test this difference, two run-tests have been performed using the difference between each point and an average curve, both along the *X*- and the *Y*-directions. These run-tests were performed on individual data points and the chosen average curve was $W5 = 1.5 \cdot T^{0.5}$ (corresponding roughly to the trend found for the whole database; Fig. 6). The populations were clearly different with 99.5% confidence along *X* and 95% confidence along *Y*. These results confirm the general asymmetry of the damage zone observed from field and experimental examples, but no distinction could be identified between the two sides in terms of deformation band density. This implies that although damage zones may be wider in the hanging wall side of faults, their maximum deformation intensity (strain) is comparable on both sides of the fault.

4.2. Fault-related folding

Fault-related folding of the bedding within the damage zone appears to significantly influence the average deformation band density. To explore this relationship we have grouped our limited data into folded (drag or rollover) and non-folded damage zones. As a first approach, the arithmetic mean of the average densities *D*5 was calculated for damage zones associated with faults with a small throw (below 10 m) versus a large throw (larger than 100 m) (Fig. 13A). The results (Fig. 12A) suggest that folding has no influence on damage zones associated with small throws. The average density *D*5 is between 15 and 22 deformation bands per meter. In contrast, for larger throws, the average density triples for the dragged damage zones as compared to the non-folded damage zones (Fig. 13A). However, since only three data points support this observation, no firm conclusion can be drawn. In a further attempt

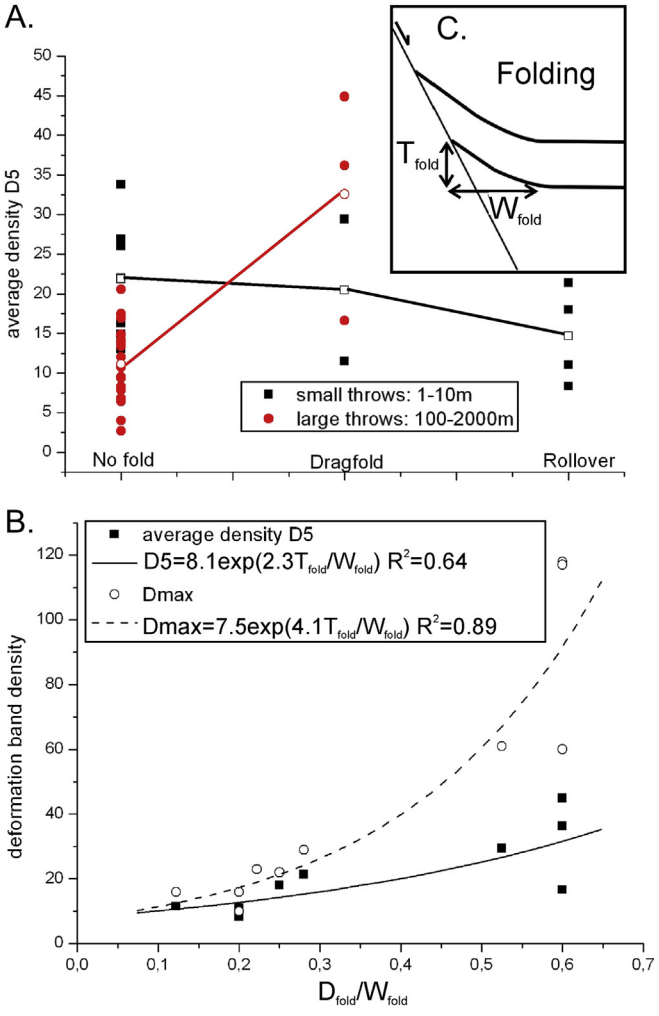

Fig. 13. A) Average density of deformation bands for non-folded and folded (rollover or dragfold) damage zones. Only damage zones associated with faults having a throw of 1–10 m and larger than 100 m have been analyzed. B) Average density *D*5 and maximum density *D*max as a function of the ratio *T*fold/*W*fold. C) Illustration of *T*fold and *W*fold as applied in the analysis of "B". *T*fold is the displacement accommodated by the fold and *W*fold is the length other which the layer is considered as folded.

to test the influence of the degree of folding on the damage zone, we define the two parameters *T*fold, which is the throw accommodated by the fold, and *W*fold, which is the horizontal distance over which the folding takes place, i.e. the width of the drag or rollover fold. Hence, the ratio *T*fold/*W*fold is a measure of fold curvature. A correlation between the average deformation band density of the folded damage zones and *T*fold/*W*fold shows a positive correlation, as does maximum density versus *T*fold/*W*fold (Fig. 13B). In other words, an increase in fold curvature implies, as would be expected, a higher deformation band density.

Somewhat surprisingly, our four data points from Sinai indicate that fault-related folding does not significantly influence the width of the damage zone or the spatial distribution of the deformation bands. Slightly lower values of Dc for damage zones to large faults with folded wallrocks are observed, but this concerns values of Dc calculated on one order of magnitude length range, and the obtained average Dc value is still quite close to the global average value presented in Fig. 11. The salt-related rollover described from the Cache Valley in Arches National Park by Antonellini and Aydin (1995) may represent a counter example, suggesting that more data and further differentiation are needed to draw firm conclusions regarding the relationship between rollover structures and damage zone width.

4.3. Lithology, layer thicknesses and depth of faulting

Other parameters, such as the petrophysical properties of the host rock, layer thickness, and depth of faulting, are all likely to influence fault growth. Some analyses were performed using the database, but yielded inconclusive results. Depths of faulting varying between 0.1 and 2.5 km are represented in the database, but no specific damage zone characteristics could be related to this parameter. The density of bands seems to increase slightly with increasing grain size, based on data from the Slickrock Member (Utah) between well-sorted aeolian sandstone units and more fine-grained interdune sand units. In contrast, there seems to be a relationship between the average permeability (and porosity) values of the host-rock and the average density of deformation bands in the damage zone, emphasizing that the average densities in Utah sandstones (having current permeability of 0.25–3 darcy) are slightly higher than those investigated in Sinai (currently around 10 darcy). Again, no statistically valid conclusions can be established, and more data are needed to explore the lithologic and petrophysical effects on damage zone characteristics.

Since most of the data come from Utah or Egypt, these two subpopulations have been compared in Fig. 14. The damage zone width (*W*5)–throw (*T*) relationship is quite similar for both subpopulations. The really large fault throws existing only in the Egypt subpopulation have been removed for the comparison. The correlation dimension Dc is also quite similar for both subpopulations (0.84 for Egypt and 0.85 for Utah). Only the average density *D*5 is slightly larger for the Utah subpopulation (16.3 deformation bands per meter) than the Egypt subpopulation (11.5 deformation bands per meter). These comparisons indicate that the results (mainly the width–throw relationship and the clustering of the deformation bands) are independent on the locality and are thus robust.

5. Deterministic statistical model for damage zone growth

The growth history of a damage zone as the related fault accumulates displacement is not well understood. Our database is sufficiently large to model this aspect to some extent based on statistics alone. We define a simple deterministic statistical model

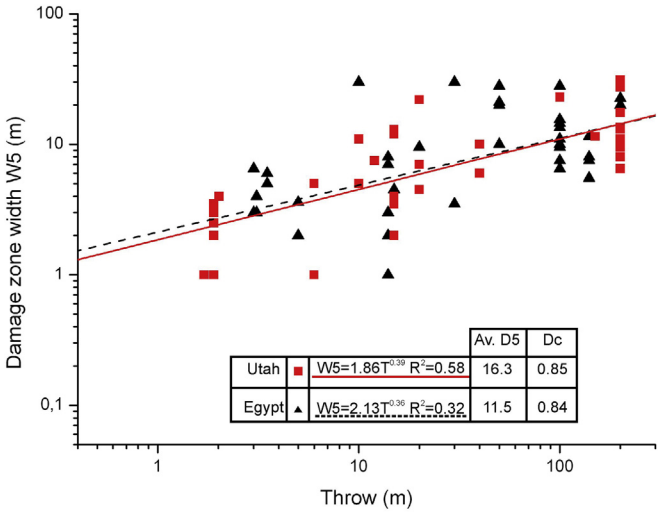

Fig. 14. Damage zone width *W*5 as a function of throw (*T*) for only Utah (squares) and Egypt (triangles) damage zones. The table gives the principal characteristics for the two groups of damage zones. Av. *D*5 is the average damage density of deformation bands in the damage zone calculated up to a width *W*5. Dc is the average correlation dimension.

by imposing some probabilistic rules based on the observations defined from the database, as discussed in the previous section. The following rules are applied:

- We impose the increase of the fault throw so that the width of the damage zone is imposed and increases by 1 m at each step of the calculation. However, we do not try to mimic the real timing of fault and damage zone growth.
- We impose a constant average density of deformation bands in the damage zone. Here we choose $D5 = 12$ deformation bands per meter.
- The width ($W5$) and the average density ($D5$) allow us to define the parameters of the logarithmic decrease (A and L).

$$A = \frac{D5 \times W5 \times \ln(W5) - 5\sum_{i=1-0,5}^{W5-0,5} \ln(i)}{W5 \times \ln(W5) - \sum_{i=1-0,5}^{W5-0,5} \ln(i)}$$

$$L = \frac{5 - A}{\ln(W5)}$$

- Finally, in line with our results, we assume that the clustering of deformation bands as expressed by Dc remains stable during the fault damage zone growth. We choose a Dc value equal to 0.84.
- In order to define the fractal distribution of deformation bands in 1D, we use the multiplicative cascade algorithm defined in Darcel (2002). The method is also used in Du Bernard et al. (2002).

By combining Dc, A and L, an ideal frequency graph can be calculated for each step of the damage zone growth. This frequency graph (deformation band density value as a function of the distance from the fault core) corresponds to the best combination of deformation band frequency satisfying the clustered distribution (and Dc value) and the logarithmic decrease described by A and L.

A last constraint is added to the model: any cluster of deformation bands that exists at a given step should still exist at the following step, i.e., the frequency of deformation bands observed at a certain distance in the damage zone cannot decrease in the next step, when the damage zone width increases. Fig. 15A shows the evolution of the measured width (using *W*5) at each calculation step and its comparison with the imposed width. Each calculation step is characterized by an increase of 1 m in the input width (solid line). The real simulated width (dashed line) is not linearly increasing as imposed because of the fractal clustering component of the model. The growth of the damage zone seems to be a discontinuous process with standstill and accelerating phases, as tentatively suggested in several previous papers (e.g., Fig. 2 in Wibberley et al., 2008; Fig. 8.27 in Fossen, 2010; Braathen et al., 2013). Of course, this statistical result is independent of the real timing of the fault growth; the fault is considered here to be active and to grow continuously with time.

In Fig. 15C, the input values of A_{norma} and L_{norma}, describing the logarithmic decrease of the deformation bands frequency away from the fault core, as well as the measured ones, are plotted. While it was not possible to define a trend using the database values (light gray squares, same as in Fig. 9D), the probabilistic model (colored points) suggests that L_{norma} increases slightly with increasing damage zone width.

The damage zone width can be related to the fault throw using the relationships defined in Fig. 6 or Fig. 12. Fig. 16 illustrates the growth of a damage zone obtained with the probabilistic model. Each step corresponds to an increase of the input damage zone width *W*5 of 5 m. The yellow/light color in the frequency graphs corresponds to existing deformation band frequency at the last step, whereas the green/dark color corresponds to the newly formed deformation bands.

By applying these simple statistical rules, we are able to generate frequency graphs that are coherent with observations performed on outcrop. The "statistical growth" of the damage zone is characterized by the creation of new deformation bands both within and outside the existing damage zone. Noticeably, following these statistical rules, it is impossible to grow a damage zone by only adding new deformation bands outside the existing damage zone. It is also interesting to note that the maximum frequency of deformation bands (*D*max) rapidly reaches a high value (increases up to 40 deformation bands per meter for a width between 2 and 25 m – for increasing throw from 2 to 280 m) and then stabilizes (between 40 and 50 deformation bands per meter for widths between 25 and 50 m – throw between 280 and 1100 m) (Fig. 15B). This is not a parameter constrained by the model and such a limitation of the maximum observed density seems thus only constrained by the statistical distribution of the deformation bands in the damage zone.

6. Discussion – implications for damage zone development

Our study corroborates the generally accepted positive correlation between fault throw and damage zone thickness, and presents quantified estimates for this relationship for normal fault in porous sandstones (Fig. 6). The relationship between fault throw and damage zone width has been described in various ways by previous authors. While some favor a linear relationship between damage zone width and fault throw measured along a single fault (Knott et al., 1996; Shipton and Cowie, 2001) or a partially linear relationship depending on the location along the fault (Savage and Brodsky, 2011), others define non-linear trends (Beach et al., 1997, 1999; Fossen and Hesthammer, 2000). In general the widening of the damage zone is attributed to shearing and attrition of fault wall rock (Robertson, 1983; Scholz, 1987; Power et al., 1988) or

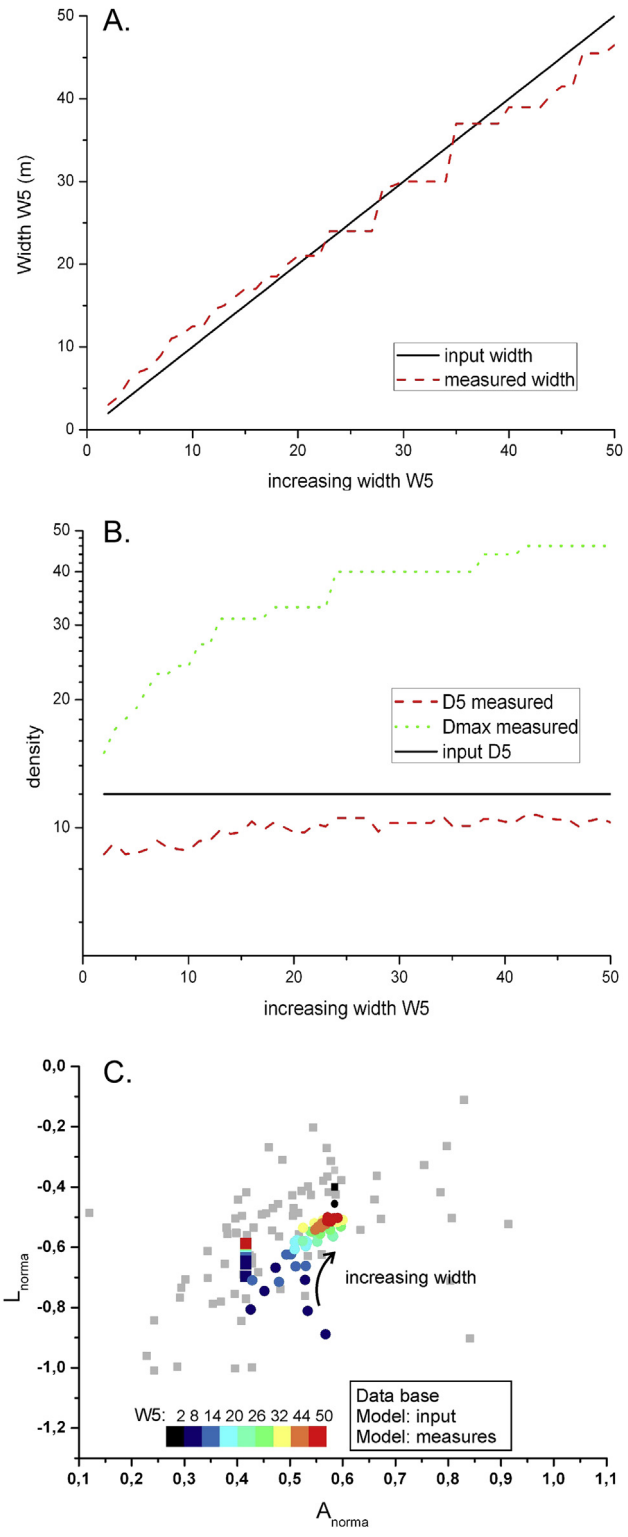

Fig. 15. A) Evolution of the simulated damage zone width (*W*5 – dashed line) with increasing input width (solid line – slope of 1). The input width is increasing by 1 m for each calculation step. B) Evolution of the simulated average density (*D*5 – dashed line) and of the maximum density (*D*5max – dotted line) with increasing input width. The solid line corresponds to the input density equal to 12 deformation bands per meter. C) A_{norma}–L_{norma} plot: the light gray squares corresponds to the data points (same as in Fig. 9B). The square points represent A_{norma} and L_{norma} calculated using the input values, and the round points correspond to A_{norma} and L_{norma} measured on the different scanlines obtained from the simulation. Note that L_{norma} is increasing with increasing input width *W*5 (see color scale for value of *W*5).

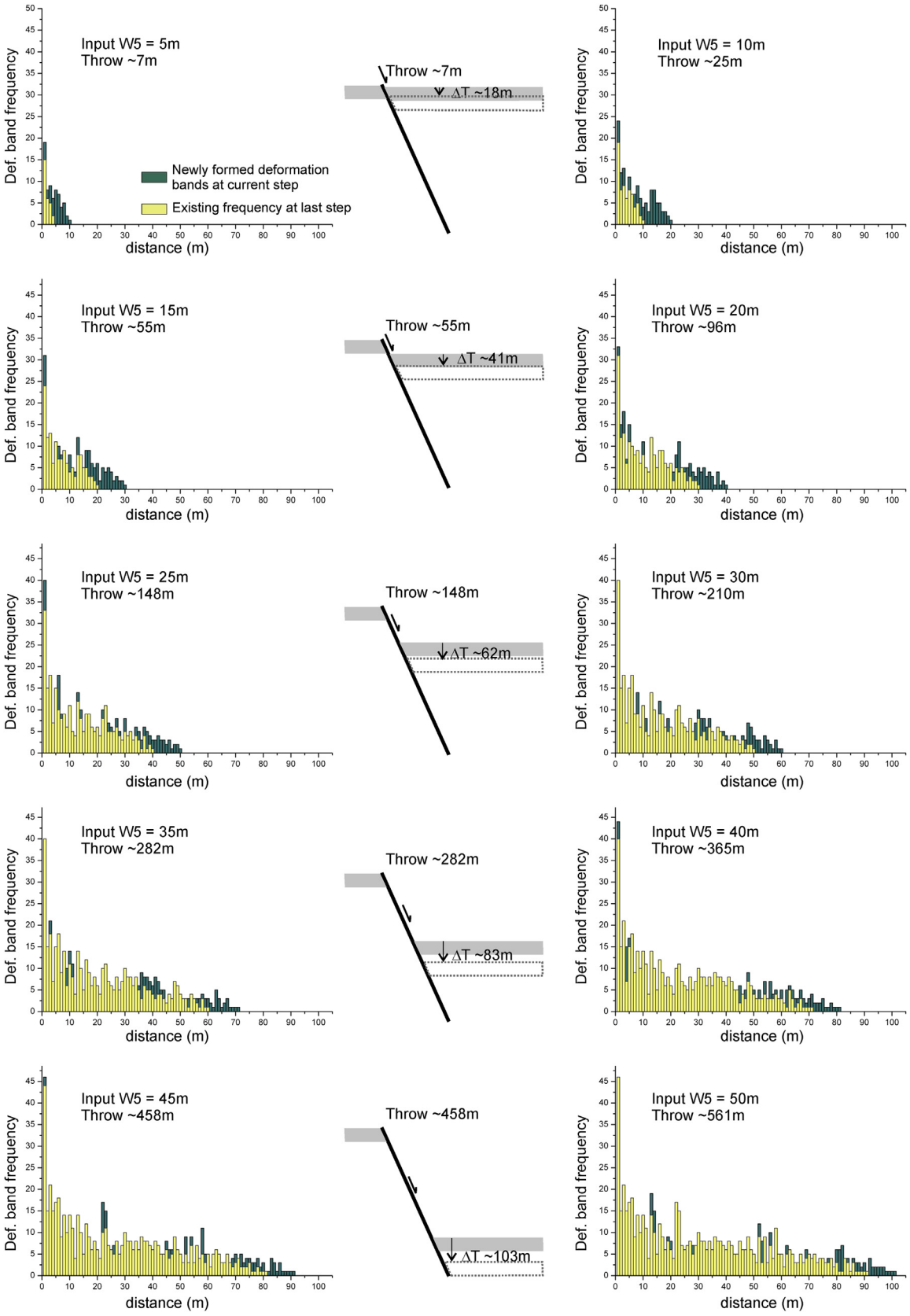

Fig. 16. Illustration of damage zone evolution with fault throw increase applying the numerical model established for deformation band distribution. At each step, the light colored bars of the frequency graphs correspond to the existing deformation band frequency at the previous step, and the dark colored bars correspond to the newly formed deformation bands. The throw is deduced from the input $W5$ using the following formula: $W5 = 1.86 \cdot T^{0.52}$ (defined for hanging wall damage zone in Fig. 12). The indicated throw corresponds to the damage zone width given on the left graph and ΔT defines the added throw to reach the damage zone width given in the right graph.

strain hardening of fault rocks (Hull, 1988; Faulkner et al., 2003; Kaproth et al., 2010). A number of authors (e.g., Rykkelid and Fossen, 2002; Fossen et al., 2007; Wibberley et al., 2008; Childs et al., 2009) also point out that the thickness and distribution of fault-related deformation are largely influenced by fault geometry and more specifically by the locations and dimensions of steps or bends of the fault surface produced during fault propagation, which would account for the observed variability in damage zone widths in this dataset. That is why we focused here on individual fault segments in order to reduce, if not eliminate, this source of variability.

The decrease of the deformation away from the fault core follows a logarithmic decrease in most of our measured damage zones, as shown in Fig. 9, which is also supported by observations of the density of fabric elements in damage zones both of mesoscopic structures and micro-fractures (Anders and Wiltschko, 1994; Scholz et al., 1993; Vermilye and Scholz, 1998; Chester et al., 2004). In other cases, the deformation band or (micro) fracture density has been ascribed to an exponential decay as a function of the distance from the fault surface, for example in the Navajo and Entrada sandstones in Arches National Park (Anders and Wiltschko, 1994), and in the granodiorite and diorite of the Atacama fault system (Mitchell and Faulkner, 2009). Savage and Brodsky (2011) modeled the fracture density decay by a power law in order to mimic the power law decay of stress produced from a line or a point source, but the correlation coefficients calculated using logarithmic decay for these data are not necessarily worse than for power-law or exponential decay.

The previous observations and statistical characteristics offer insight into damage zone growth around normal faults in porous sandstones. Starting with Aydin and Johnson (1978), deformation band formation causes strain hardening, while subsequent slip surface faulting is related to strain softening in the same rocks. This raises the questions why deformation bands continue to develop after the establishment of a weak and continuous slip surface that can accommodate large displacements and relax the surrounding stress. Variation in deformation band density around the slip surface is, however, considerable. Damage zones clearly grow as demonstrated by all the positive correlations defined between the damage zone width and the accumulated throw along faults (Fig. 16).

Renewed deformation band growth could be related to establishment of fault lenses or geometrical asperities along the slip surface, obstacles that cause localized stress concentration along the fault. The model of Aydin (1978) and Aydin and Johnson (1978) predicts that faults in porous sandstones grow from swarms of deformation bands. This model explains why deformation bands never accumulate more than cm-scale displacements before interlocking of grains that causes strain to delocalize by the formation of new band in the vicinity. According to the observations and the probabilistic model established in this study, new deformation bands do not necessarily form in the close vicinity of an existing cluster; new clusters can form outside of the established damage zone (as advocated by Saillet and Wibberley, 2010), while the existing clusters may continue to grow. Nevertheless, according to the fault growth model of Scholz et al. (1993) or Vermilye and Scholz (1998), a damage zone (or process zone) exists prior to the formation of the slip surface. Our analysis shows that there is no statistically significant correlation between fault throw and the maximum density of deformation bands. Furthermore, the fact that clusters close to the fault core have similar observed maximum deformation band densities in both wide and narrow damage zones (Fig. 16) suggests that a maximum density of deformation bands (per meter) is rapidly established in the damage zone during fault evolution.

We propose that the maximum band density may be linked to a critical stress level at which the clusters become saturated with deformation bands. In highly porous aeolian sandstones, the maximum observed deformation band density ranges from 25 to 60 deformation bands per meter, but may be as high as 100 per meter (Johansen and Fossen, 2008) (values a bit more scattered in Fig. 8B). Interestingly, this characteristic geometry is also observed in our probabilistic model, where no upper limit has been fixed (Fig. 16). In the latter case, the limitation of the density value is reproduced by the spatial distribution of the deformation bands and the geometry of the damage zone. The fact that the frequency of deformation bands is more or less constant during damage zone growth and thus independent of fault throw indicates that the formation of new clusters and maturation of existing clusters within the developing damage zone is more or less coeval. This result points out a scale invariant damage zone growth, where the creation of new deformation bands is balanced by the widening of the damage zone.

Higher density or a higher scatter in orientation of deformation bands may result from mechanical interaction associated with fault branch points, fault overlap zones and fault intersections. Such structural complexities are a prerequisite to accommodate differences in kinematics of interacting faults (Cruikshank et al., 1991; Childs et al., 1995; Davatzes et al., 2005; Johansen et al., 2005). The effects of structural complexities, orientations and lengths have not been analyzed in this study since only single fault segments were taken into account.

All of our data were collected from highly porous and permeable sandstones. However, these sandstones show significant differences in grain size, grain sorting and state of lithification. Accordingly, the documented robust damage zone throw-width trends documented in this work attest to a global mechanism for damage zone growth, in which lithology and sedimentary facies seems to be of subordinate importance. Other factors, such as the position in the footwall or hanging wall, and maybe fault zone folding, are factors of more significance (see also the example of the Berge fault damage zone in Kvamshesten basin; Braathen et al., 2013). We advocate that a global scaling of the damage zone width with fault displacement can be identified. Similarly, the distribution of the deformation bands remains spatially self-similar during the fault zone evolution.

7. Conclusions

The presented outcrop-based database of damage zones of normal faults in porous siliciclastic sediments consists of 106 scanlines perpendicular to fault strike. The scanlines record the distribution of deformation bands in the damage zone. Analysis of the database identifies the following characteristics of damage zones in porous sandstones:

1. The damage zone width scales with the throw of the corresponding fault. The relationship between damage zone width and throw is a non-linear relationship, corresponding to a power-law with an exponent close to 0.5.
2. The damage zone is statistically wider in the hanging wall than the footwall.
3. The density of deformation bands in the damage zone is more or less independent of the throw. An average value of 15 m^{-1} is defined, even if the range of values is large (between 5 and 25 m^{-1}). Larger densities of deformation bands are observed in folded damage zones.
4. There is an overall logarithmic decrease in the frequency of deformation bands away from the fault core.

5. Deformation bands in the damage zone are spatially clustered and their position along a scanline can be described by a fractal distribution with a correlation dimension equal to 0.84, irrespective of the displacement on the fault.

These observations imply that the fault growth can be considered as a scale invariant process. A process zone already exists before the onset of the fault slip plane. With localized fault slip, the damage zone is growing. Growth is characterized by a constant balance between the development of new deformation bands in the existing damage zone and new bands exterior to this zone, leading to combined and probably stepwise increase in deformation band frequency and widening of the damage zone. The distribution of the deformation bands in the damage zone is spatially self-similar throughout the fault evolution.

Acknowledgments

This research was supported by VISTA, the research project of Statoil, as a post-doctoral grant for the first author, and is part of the Fault Facies Project at UNI CIPR.

Thanks to Harmon Maher and the two reviewers, who greatly helped to improve the manuscript by judicious comments.

References

Aarland, R.-K., Skjerven, J., 1998. Fault and fracture characteristics of a major fault zone in the northern North Sea: analysis of 3D seismic and oriented cores in the Brage Field (Block 31/4). In: Coward, M.P., Johnson, H., Daltaban, T.S. (Eds.), Structural Geology in Reservoir Characterization. Geological Society Special Publication, London, vol. 127, pp. 209–229.

Anders, M.H., Wiltschko, D.V., 1994. Microfracturing, paleostress and the growth of faults. Journal of Structural Geology 16, 795–815.

Antonellini, M.A., Aydin, A., 1994. Effect of faulting on fluid flow in porous sandstones: petrophysical properties. AAPG Bulletin 78, 355–377.

Antonellini, M.A., Aydin, A., 1995. Effect of faulting on fluid flow in porous sandstones: geometry and spatial distribution. AAPG Bulletin 79, 642–671.

Antonellini, M.A., Aydin, A., Pollard, D.D., 1994. Microstructures of deformation bands in porous sandstones at Arches national Park, Utah. Journal of Structural Geology 16, 941–959.

Antonellini, M.A., Pollard, D.D., 1995. Distinct element modeling of deformation bands in sandstone. Journal of Structural Geology 17, 1165–1182.

Aydin, A., 1978. Small faults formed as deformation bands in sandstone. Pure and Applied Geophysics 116, 913–930.

Aydin, A., Johnson, A.M., 1978. Development of faults as zones of deformation bands and slip surfaces in sandstone. Pure and Applied Geophysics 116, 931–942.

Aydin, A., Johnson, A.M., 1983. Analysis of faulting in porous sandstones. Journal of Structural Geology 5, 19–31.

Beach, A., Brown, L.J., Welbon, A.W., McCallum, J.E., Brockbank, P.J., Knott, S.D., 1997. Characteristics of faults zones in sandstones from NW England: application to fault transmissivity. In: Meadows, N.S., Trueblood, S.P., Hardman, R., Cowan, G. (Eds.), Petroleum Geology of the Irish Sea and Adjacent Areas. Geological Society Special Publication, London, vol. 124, pp. 315–324.

Beach, A., Welbon, A.I., Brockbank, P.J., McCallum, J.E., 1999. Reservoir damage around faults: outcrop examples from the Suez rift. Petroleum Geoscience 5, 109–116.

Bense, V.F., Berg, E.H.V.D., Balen, R.T.V., 2003. Deformation mechanisms and hydraulic properties of fault zones in unconsolidated sediments; the Roer Valley Rift System, The Netherlands. Hydrogeology Journal V11, 319–332.

Berg, S.S., Skar, T., 2005. Controls on damage zone asymmetry of a normal fault zone: outcrop analyses of a segment of the Moab fault, SE Utah. Journal of Structural Geology 27, 1803–1822.

Bonnet, E., Bour, O., Davy, P., Main, I.G., Cowie, P.A., Berkowitz, B., 2001. Scaling of fracture systems in geological media. Reviews of Geophysics 39, 347–383. http://dx.doi.org/10.1029/1999RG000074.

Brogi, A., 2008. Fault zone architecture and permeability features in siliceous sedimentary rocks: insights from the Rapolano geothermal area (Northern Apennines, Italy). Journal of Structural Geology 30, 237–256.

Braathen, A., Osmundsen, P.T., Hauso, H., Semshaug, S., Fredman, N., Buckley, S.J., 2013. Fault-induced deformation in a poorly consolidated, siliciclastic growth basin: a study from the Devonian in Norway. Tectonophysics 586, 112–129.

Braathen, A., Tveranger, J., Fossen, H., Skar, T., Cardozo, N., Semshaug, S., Bastesen, E., Sverdrup, E., 2009. Fault facies as concept and its applications to sandstone reservoirs. AAPG Bulletin 93, 891–917.

Caine, J.S., Evans, J.P., Forster, C.B., 1996. Fault zone architecture and permeability structure. Geology 24, 1025–1028.

Chester, F.M., Chester, J.S., Kirschner, D.L., Schulz, S.E., Evans, J.P., 2004. Structure of large-displacement, strike-slip fault zones in the brittle continental crust. In: Karner, G.D., Taylor, B., Driscoll, N.W., Kohlstedt, D.L. (Eds.), Rheology and Deformation of the Lithosphere at Continental Margins. Columbia University Press, New York, pp. 223–260.

Chester, F.M., Evans, J.P., Biegel, R.L., 1993. Internal structure and weakening mechanisms of the San Andreas fault. Journal of Geophysical Research 98, 771–786.

Chester, F.M., Logan, J.M., 1987. Composite planar fabric of gouge from the Punchbowl fault. Journal of Structural Geology 9, 621–634.

Childs, C., Manzocchi, T., Walsh, J.J., Bonson, C.G., Nicol, A., Schöpfer, M.P.J., 2009. A geometric model of fault zone and fault rock thickness variations. Journal of Structural Geology 31, 117–127. http://dx.doi.org/10.1016/j.jsg.2008.08.009.

Childs, C., Watterson, J., Walsh, J.J., 1995. Fault overlap zones within developing normal fault systems. Journal of the Geological Society, London 152, 535–549.

Cloos, E., 1968. Experimental analysis of Gulf Coast fracture patterns. AAPG Bulletin 52, 420–441.

Cruikshank, K.M., Zhao, G., Johnson, A.M., 1991. Analysis of minor fractures associated with joints and faulted joints. Journal of Structural Geology 13, 865–886.

Darcel, C., 2002. Corrélations dans les réseaux de fractures: caractérisation et conséquences sur les propriétés hydrauliques. Université de Rennes 1, France.

Davatzes, N.C., Eichhubl, P., Aydin, A., 2005. The structural evolution of fault zones in sandstone by multiple deformation mechanisms: Moab Fault, SE Utah. Geological Society of America Bulletin 117, 135–148.

Dor, O., Rockwell, T.K., Ben-Zion, Y., 2006. Geological observations of damage asymmetry in the structure of the San Jacinto, San Andreas and Punchbowl faults in southern California: a possible indicator for preferred rupture propagation direction. Pure and Applied Geophysics 163, 301–349. http://dx.doi.org/10.1007/s00024-005-0023-9.

Dor, O., Yildrim, C., Rockwell, T.K., Ben-Zion, Y., Emre, O., Sisk, M., Duman, T.Y., 2008. Geologic and geomorphologic asymmetry across the rupture zone of the 1943 and 1944 earthquakes on the North Anatolian fault: possible signals for preferred earthquake propagation direction. Geophysical Journal International 173, 483–504. http://dx.doi.org/10.1111/j.1365-246X.2008.03709.x.

Du Bernard, X., Labaume, P., Darcel, C., Davy, P., Bour, O., 2002. Cataclastic slip band distribution in normal fault damage zones, Nubian sandstones, Suez rift. Journal of Geophysical Research 107, 2141.

Ehrlich, R., 2003. The Structural Deformation in Hangingwalls of Extensional Ramp-flat-ramp Faults. University of Bergen.

Faulkner, D.R., Lewis, A.C., Rutter, E.H., 2003. On the internal structure and mechanics of large strike-slip fault zones: field observations of the Carboneras fault in southeastern Spain. Tectonophysics 367, 235–251.

Faulkner, D.R., Mitchell, T.M., Jensen, E., Cembrano, J., 2011. Scaling of fault damage zones with displacement and the implications for fault growth processes. Journal of Geophysical Research 116, B05403.

Fisher, Q.J., Knipe, R.J., 2001. The permeability of faults within siliciclastic petroleum reservoirs of the North Sea and Norwegian Continental Shelf. Marine and Petroleum Geology 18, 1063–1081.

Flodin, E.A., Prasad, M., Aydin, A., 2003. Petrophysical constraints on deformation styles in Aztec Sandstone, southern Nevada, USA. Pure and Applied Geophysics 160, 1589–1610.

Fossen, H., 2010. Structural Geology. Cambridge University Press.

Fossen, H., Bale, A., 2007. Deformation bands and their influence on fluid flow. AAPG Bulletin 91, 1685–1700.

Fossen, H., Hesthammer, J., 1997. Geometric analysis and scaling relations of deformation bands in porous sandstone. Journal of Structural Geology 19, 1479–1493.

Fossen, H., Hesthammer, J., 1998. Structural geology of the Gullfaks Field, northern North Sea. In: Coward, M.P., Johnson, H., Daltaban, T.S. (Eds.), Structural Geology in Reservoir Characterization. Geological Society Special Publication, London, vol. 127, pp. 231–261.

Fossen, H., Hesthammer, J., 2000. Possible absence of small faults in the Gullfaks Field, northern North Sea: implications for downscaling of faults in some porous sandstones. Journal of Structural Geology 22, 851–863.

Fossen, H., Johansen, T.E.S., Rotevatn, A., Hesthammer, J., 2005. Fault interaction in porous sandstones. AAPG Bulletin 89, 1593–1606.

Fossen, H., Schultz, R.A., Shipton, Z.K., Mair, K., 2007. Deformation bands in sandstone: a review. Journal of the Geological Society, London 164, 755–769.

Gjessen, T., 2001. Hvordan ulike litologier kan bidra til forkastningsforsegling-Observasjoner fra sedimentære bergarter av karbon alder i Northumberland, nordøst England. University of Bergen.

Grassberger, P., Procaccia, I., 1983. Measuring the strangeness of strange attractors. Physica D 9, 189–208.

Hesthammer, J., Fossen, H., 2001. Structural core analysis from the Gullfaks area, northern North Sea. Marine and Petroleum Geology 18, 411–439. http://dx.doi.org/10.1016/S0264-8172(00)00068-4.

Hull, J., 1988. Thickness-displacement relationships for deformation zones. Journal of Structural Geology 10, 431–435.

Jamison, W.R., Stearns, D.W., 1982. Tectonic deformation of Wingate sandstone, Colorado National Monument. Bulletin of the American Association of Petroleum Geologists 66, 2584–2608.

Johansen, T.E.S., Fossen, H., 2008. Internal geometry of fault damage zones in interbeded siliciclastic sediments. In: Wibberley, C.A.J., Kurz, W., Imber, J., Holdsworth, R.E., Collettini, C. (Eds.), The Internal Structure of Fault Zones: Implications for Mechanical and Fluid-flow Properties. The Geological Society of London, London, vol. 299, pp. 35–56.

Johansen, T.E.S., Fossen, H., Kluge, R., 2005. The impact of syn-faulting porosity reduction on damage zone architecture in porous sandstone: an outcrop example from the Moab Fault, Utah. Journal of Structural Geology 27, 1469–1485.
Johnson, A.M., 1995. Orientations of faults determined by premonitory shear zones. Tectonophysics 247, 161–238.
Kaproth, B.M., Cashman, S.M., Marone, C., 2010. Deformation band formation and strength evolution in unlithified sand: the role of grain breakage. Journal of Geophysical Research 115. http://dx.doi.org/10.1029/2010JB007406.
Kim, Y.-S., Peacock, D.C.P., Sanderson, D.J., 2004. Fault damage zones. Journal of Structural Geology 26, 503–517. http://dx.doi.org/10.1016/j.jsg.2003.08.002.
Knott, S.D., Beach, A., Brockbank, P.J., Lawson Brown, J., McCallum, J.E., Welbon, A.I., 1996. Spatial and mechanical controls on normal fault populations. Journal of Structural Geology 18, 359–372.
Kolyukhin, D., Schueller, S., Espedal, M.S., Fossen, H., 2009. Deformation band populations in fault damage zone – impact on fluid flow. Computational Geosciences. http://dx.doi.org/10.1007/s10596-009-9148-8.
Lockner, D.A., Tanaka, H., Ito, H., Ikeda, R., Omura, K., Naka, H., 2009. Geometry of the Nojima fault at Nojima-Hirabayashi, Japan. I. A simple damage structure inferred from borehole core permeability. Pure and Applied Geophysics 166, 1649–1667. http://dx.doi.org/10.1007/s00024-009-0515-00020.
Mair, K., Main, I., Elphick, S., 2000. Sequential growth of deformation bands in the laboratory. Journal of Structural Geology 22, 25–42.
McClay, K., Scott, A.D., 1991. Experimental models of hangingwall deformation in ramp-flat listric extensional fault systems. Tectonophysics 188, 85–96.
McGrath, A.G., Davison, A.G., 1995. Damage zone geometry around fault tips. Journal of Structural Geology 17, 1011–1024.
Menendez, B., Zhu, W., Wong, T.-F., 1996. Micromechanics of brittle faulting and cataclastic flow in Berea sandstone. Journal of Structural Geology 18, 1–16.
Micarelli, L., Moretti, I., Daniel, J.-M., 2003. Structural properties of rift-related normal faults: the case study of the Gulf of Corinth, Greece. Journal of Geodynamics 36, 275–303. http://dx.doi.org/10.1016/S0264-3707(03)00051-6.
Mitchell, T.M., Faulkner, D.R., 2009. The nature and origin of off-fault damage surrounding strike-slip fault zones with a wide range of displacements: a field study from the Atacama fault system, northern Chile. Journal of Structural Geology 31, 802–816. http://dx.doi.org/10.1016/j.jsg.2009.05.002.
Peacock, D.C.P., Knipe, R.J., Sanderson, D.J., 2000. Structural geology: glossary of normal faults. Journal of Structural Geology 22, 291–305.
Power, W.L., Tullis, T.E., Weeks, J.D., 1988. Roughness and wear during brittle faulting. Journal of Geophysical Research 93, 15268–15278. http://dx.doi.org/10.1029/JB093iB12p15268.
Powers, P.M., Jordan, T.H., 2010. Distribution of seismicity across strike-slip faults in California. Journal of Geophysical Research 115. http://dx.doi.org/10.1029/2008JB006234.
Robertson, E.C., 1983. Relationship of fault displacement to gouge and breccia thickness. Mining Engineering 35, 1648–1662.
Rotevatn, A., Fossen, H., 2011. Simulating the effect of subseismic fault tails and process zones in a siliciclastic reservoir analogue: implications for aquifer support and trap definition. Marine and Petroleum Geology 28, 1648–1662.
Rykkelid, E., Fossen, H., 2002. Layer rotation around vertical fault overlap zones: observations from seismic data, field examples, and physical experiments. Marine and Petroleum Geology 19, 181–192. http://dx.doi.org/10.1016/SG0264-8172(02)00007-7.
Saillet, E., Wibberley, C.A.J., 2010. Evolution of cataclastic faulting in high-porosity sandstone, Bassin du Sud-Est, Provence, France. Journal of Structural Geology 32, 1590–1608. http://dx.doi.org/10.1016/j.jsg.2010.02.007.
Savage, H.M., Brodsky, E.E., 2011. Collateral damage: evolution with displacement of fracture distribution and secondary fault strands in fault damage zones. Journal of Geophysical Research 116. http://dx.doi.org/10.1029/2010JB007665.
Scholz, C.H., 1987. Wear and gouge formation in brittle faulting. Geology 15, 493–495.
Scholz, C.H., Dawers, N.H., Yu, J.Z., Anders, M.H., Cowie, P.A., 1993. Fault growth and fault scaling laws: preliminary results. Journal of Geophysical Research 98, 21.951–21.961.
Schultz, R.A., Siddharthan, R., 2005. A general framework for the occurrence and faulting of deformation bands in porous granular rocks. Tectonophysics 411, 1–18. http://dx.doi.org/10.1016/j.tecto.2005.07.008.
Schulz, S.E., Evans, J.P., 1998. Spatial variability in microscopic deformation and composition of the Punchbowl fault, southern California: implications for mechanisms, fluid-rock interaction and fault morphology. Tectonophysics 295, 223–244.
Shipton, Z.K., Cowie, P.A., 2001. Damage zone and slip-surface evolution over [mu]m to km scales in high-porosity Navajo sandstone, Utah. Journal of Structural Geology 23, 1825–1844.
Shipton, Z.K., Cowie, P.A., 2003. A conceptual model for the origin of fault damage zone structures in high-porosity sandstone. Journal of Structural Geology 25, 333–344.
Shipton, Z.K., Soden, A.M., Kirkpatrick, J.D., Bright, A.M., Lunn, R.J., 2006. How thick is a fault? Fault displacement – thickness scaling revisited. In: Abercrombie, R.E., McGarr, A., Kanamori, H., Di Toro, G. (Eds.), Earthquakes: Radiated Energy and the Physics of Faulting. Geophysical Monograph Series, vol. 170. The American Geophysical Union.
Torabi, A., Fossen, H., 2009. Spatial variation of microstructure and petrophysical properties along deformation bands in reservoir sandstones. AAPG Bulletin 93, 919–938. http://dx.doi.org/10.1306/03270908161.
Underhill, J.R., Woodcock, N.H., 1987. Faulting mechanisms in high-porosity sandstones: New Red Sandstone, Arran, Scotland. In: Jones, M.E., Preston, R.M.F. (Eds.), Deformation of Sediments and Sedimentary Rocks. The Geological Society of London, vol. 91–105.
Vermilye, J.M., Scholz, C.H., 1998. The process zone: a microstructural view of fault growth. Journal of Geophysical Research 103, 12,223–12,237.
Vicsek, T., 1989. Fractal Growth Phenomena. World Sci., River Edge, N.J.
Wallace, R.E., Morris, H.T., 1979. Characteristics of Faults and Shear Zones as Seen in Mines at Depths as Much as 2.5 km Below the Surface. United States Geological Survey Open File Report 79-1239, pp. 79–100.
Wibberley, C.A.J., Yielding, G., Di Toro, G., 2008. Recent advances in the understanding of fault zone internal structure: a review. In: Wibberley, C.A.J., Kurz, W., Imber, J., Holdsworth, R.E., Collettini, C. (Eds.), The Internal Structure of Fault Zones: Implications for Mechanical and Fluid-flow Properties. Geological Society Special Publication, London, vol. 299, pp. 5–33.
Withjack, M.O., Islam, Q.T., Lapointe, P.R., 1995. Normal faults and their hangingwall deformation – an experimental study. AAPG Bulletin 79, 1–18.